Received: 31 October 2016 | Revised: 8 October 2017 | Accepted: 12 January 2018

DOI: 10.1111/exsy.12270

ORIGINAL ARTICLE

WILEY Expert Systems

Advances in multisensor information fusion: A Markov–Kalman viscosity fuzzy statistical predictor for analysis of oxygen flow, diffusion, speed, temperature, and time metrics in CPAP

James A. Rodger[1,2]

[1] MIS and Decision Sciences, Indiana University of Pennsylvania, Indiana, Pennsylvania, USA

[2] ISDS, Hooversville, Pennsylvania, USA

Correspondence
James A. Rodger, MIS and Decision Sciences, Indiana University of Pennsylvania, 203 M ECOBIT 774 Pratt Drive, Indiana, Pennsylvania 15705, USA.
Email: jrodger@iup.edu

Abstract

The efficacies of continuous positive airway pressure (CPAP) are well documented in decreasing the apnoea–hypopnoea index in patients with obstructive sleep apnoea. To guarantee these efficacies, CPAP manufacturers must thoroughly test these devices to ensure the flow of oxygenated air to the patient at various temperatures during a prescribed time frame. The calculation of the percent oxygen in a "bimixture" of gas can be done by measuring the travel time of a sound wave through the gas, and the travel time is proportional to the density of the air. We utilized existing multisensor tubes that were developed to collect and measure oxygen flow, diffusion, speed, temperature, and time metrics. Then these metrics were analysed using a Markov fuzzy, statistical, artificial neural network, nearest-neighbour predictive approach to determine the interactions between these variables. An improved Kalman filter method was employed to reduce noise, increase viscosity, and obtain correct data from the CPAP system.

KEYWORDS

humidity, Kalman filter, multisensor coordinated monitoring, neural network, O_2 sensors, smart temperature sensor

1 | OVERVIEW AND BACKGROUND

In this article, we will introduce the problem, briefly place it in its context and antecedents, justify our objectives, and propose a solution. The problem faced is to help ensure manufacturers that continuous positive airway pressure (CPAP) devices maintain the flow of oxygenated air to the patient at various temperatures during a prescribed time frame. Our process utilized multisensory tubes to collect the data as part of an expert system. We endeavoured to place this concept in context by referring to the existing multisensory oxygen literature antecedents in Section 2. The objectives of this research are listed below, and they were met by gathering and analysing data via an improved Kalman filter method that reduced noise and increased viscosity. First, we wish to create an equation for calculating oxygen, using temperature and sound travel time as inputs. Second, we want to utilize the equation to calculate oxygen flow using temperature and sound travel time as inputs. To accomplish these tasks, we need to make some assumptions for measuring oxygen. The first assumption is that the time advance of the sound wave with flow is equivalent to the time lag of the sound wave against flow. Therefore, the average of "with" and "against" gives an equivalent time travel at 0 flow (call it AVGtime). Second, we assume that the oxygen concentration can be calculated using temperature (K) and the AVGtime. Third, we must assume that the oxygen measurement is independent of flow. We must also make some assumptions for flow. Our first assumption is that flow is proportional to the difference between the travel time of the sound wave with and against flow ($T_{\text{against}} - T_{\text{with}}$). Second, we must assume that flow measurement will be dependent on temperature. Kurtis (2016) tells us how to measure the speed of sound in a gas, because sound consists of a waveform moving through a material. We know that the speed of sound in a gas is primarily a function of the temperature of the gas. We also know that air is a mixture of gases and includes water vapour; therefore, the relative humidity of air has a slight effect on the speed of sound. However, we also know that changes in air pressure have no real effect on the speed of sound and that a simple equation can be used to approximate it. A more complex equation can also be developed to be used with other gases. The speed of sound in any gas takes into account other factors, and it is also a specific fraction of the average speed of the gas molecules at any given temperature. In our experiments, we will look at these factors

because we know that air is a relatively fixed mixture of gases, primarily consisting of nitrogen, oxygen, argon, and carbon dioxide, that includes varying amounts of water vapour or humidity. The speed of sound in air is approximately 343 m/s at room temperature (20 °C or 70 °F). This speed is primarily a function of temperature; the only other factor that has any effect on the speed of sound in air is the amount of humidity in the air. However, humidity has only a slight influence; an increase in the amount of humidity in the air increases the speed of sound by only a small amount. Humidity can vary greatly, but because the amount of change of speed with an extreme change in humidity is less than 0.5%, we can conclude that the speed of sound is usually measured in dry air, neglecting the effect of humidity. We also realize that pressure is not a factor because experiments have shown that changes in air pressure have no real effect on the speed of sound. It is also well known that sound travels slower at higher altitudes. This is because the temperature and relative humidity are lower and not because the air pressure is lower at higher altitudes. Therefore, we can calculate the speed of sound in dry air in metres per second (m/s) as being approximately equal to $v = 331.4 + 0.6TC$ m/s, where v = the speed or velocity of sound and TC is the temperature in degrees Celsius. For example, if TC = 0 °C, then $v = 331.4 + 0 = 331.4$ m/s. Similarly, if TC = 20 °C, then $v = 331.4 + 0.6 * 20 = 331.4 + 12 = 343.4$ m/s. These equations also demonstrate that as the temperature of air goes up, the speed of sound goes up concurrently.

2 | PROPOSAL ASPECTS

From the foregoing assumptions, we were able to create the equation for calculating oxygen using temperature and sound travel time as inputs. We were also able to create the equation to calculate flow using temperature and sound travel time as inputs. We know that sound travels faster in warm air. We also know that the sound speed (c) is a given designated by the equation of $c = \sqrt{(YRT/m)}$. We know that Y, R, and m are the ratio of specific heat for air, universal gas constant, and molar mass of air, respectively. Because T is the absolute temperature, R is a constant, and both Y and m are determined by the gas, then we can deduce that sound speed depends only on temperature for these purposes.

From the foregoing, we can also conclude that the speed in any gas is a function of temperature, the molecular structure of the gas, and its molecular mass. The molecular mass is the atomic weight of the molecule divided by 1,000. The speed of sound for various gases at 0 °C is as follows (in m/s): Air is 331, carbon dioxide is 259, oxygen is 316, helium is 965, and hydrogen is 1,290. We must also remember that speed is limited by the velocity of particles; with regard to the speed of sound in a gas, the speed is a distinct fraction of the average speed or velocity of the molecules or atoms making up the gas. For example, the speed of sound in air is 0.68 times the speed of the air molecules at a given temperature. In summary, the speed of sound in a gas is a function of its temperature, and air is a mixture of gases that includes water vapour. Although a simple equation can be used to approximate the speed of sound in a gas, a more complex equation is needed to take into account additional factors that can be used with other gases. We also can conclude that the speed of sound in a gas is a specific fraction of the average speed of the gas molecules at the given temperature. With these scientific aspects in place, we are now able to apply our Markov–Kalman viscosity approach, collect and analyse the data via the techniques proposed, and provide our conclusions.

3 | LITERATURE REVIEW

Distributed sensors have been proven successful for the measurement of oxygen flows and concentrations. For example, Hsieh, Cheng, Liu, and Chung (2016) studied a microbial fuel cell (MFC) biosensor inoculated with known mixed cultures to determine the biological oxygen demand (BOD) concentration. Their results indicated that monosaccharides were a good fuel for electricity generation by the MFC and that the developed MFC biosensor has great potential as an alternative BOD-sensing device for online measurements of wastewater BOD. Logroño, Guambo, Pérez, Kadier, and Recalde (2016) investigated MFCs to provide a preliminary investigation of the use of terrestrial single-chamber MFCs (SMFCs) as biosensors. Their SMFCs had good response and reproducibility as biosensor devices, and the authors found that SMFCs could be an alternative for environmental monitoring. F. Li, Wei, Chen, Li, and Zhang (2015) argued that dissolved oxygen (DO) content changes with the aquatic environment. They proposed an intelligent DO measurement method based on the fluorescence quenching mechanism and demonstrated that their optical measurement method was stable, accurate, and suitable for online DO monitoring. Guillén-Bonilla et al. (2016) used nanorods in a colloidal method and transmission electron microscopy. Their analysis revealed that the gas-sensing properties of these nanostructures possess excellent stability and high sensitivity in these atmospheres. Im, Sterner, and Swager (2016) developed an integrated sensing system, which consisted of a cellulose polymer concentrator and a single-walled carbon nanotube, to detect benzene, toluene, and xylene vapours. Their design of integrated cellulose concentrator/single-walled carbon nanotube sensing system allows high sensitivity with limits of detection for benzene, toluene, and m-xylene vapours exhibiting the potential ability for on-site, real-time sensing applications. H. Li et al. (2016) proposed a new void fraction measurement method for gas–liquid two-phase flow in small channels. A void fraction measurement system for the two-phase flow was developed, and experiments were carried out. The authors found that the measurement system was successful and compensated for the influence of the flow pattern on the void fraction measurement. The system used a low-cost laser diode as a competent replacement for the expensive standard laser source and implemented the parameter measurement of gas–liquid two-phase flow. C.-C. Chen, Chen, and Lin (2016) proposed an all-digital time-domain smart temperature sensor to linearize the curve. They achieved a new linearity-enhanced output that significantly improved temperature-sensing accuracy, avoiding costly curvature compensation. Jureschi et al. (2016) proposed a new design concept for dual-spin crossover-based sensors for concomitant detection of both temperature and pressure optimization values, identified via their optical densities, which offers great perspectives for

smart sensing devices. Cui and Murray (2015) investigated the influence of electrode configuration on the impedance metric response of nitric oxide gas sensors for solid electrochemical cells. They found that gas diffusion appeared to be a rate-limiting mechanism in sensors. When the electrode configuration resulted in longer diffusion pathways, they found that the temperature dependence of the nitric oxide sensors was independent of the electrode configuration. Stratulat et al. (2015) reported on a sonochemical synthesis method for manufacturing nanostructured powder characterized using X-ray diffraction, Mössbauer spectroscopy, and scanning electron microscopy. The oxygen sensor, based on the Sono-STFO40 sensing layer, showed good sensitivity, low power consumption (80 mW), and short response time, thus proving Sono-STFO40 to be a material suitable for oxygen detection in harsh environments. H. Wang, Chen, Wang, Sun, and Zhao (2014) developed an oxygen gas microsensor based on nanostructured sol–gel titanium oxide thin films with a buried palladium layer on a silicon substrate. This set-up showed that, after several testing cycles, the sensor's output becomes stable. The sensitivity of this arrangement has potential for application in environmental monitoring, where lower power consumption and small size are required. X. Jiang, Kim, Zhang, Johnson, and Salazar (2014) acknowledged that piezoelectric sensing is of increasing interest for high-temperature applications. They presented an overview of high-temperature piezoelectric sensing techniques in aerospace, automotive, power generation, and material processing. Løkke, Seefeldt, Edwards, and Green (2011) applied wireless sensor networks to determine the respiration rate of oxygen continuously and at modified gas compositions for the determination of oxygen and temperature in the close vicinity of the plant material. Their investigations should lead to optimized consumer products. Bahamon et al. (2011) reported on the Operational Observatory of the Catalan Sea, which provides important records on atmospheric and oceanographic conditions for this area of the Mediterranean. The Operational Observatory of the Catalan Sea has 24 moored sensors and probes, which operated in a coordinated fashion to provide data such as temperature, salinity, pressure, DO, chlorophyll fluorescence, and turbidity. The paper reported on atmospheric and oceanographic conditions, including data communication and storage. P. H. Lee and Hwang (2009) reported on the performance of fuel cell flow configuration and operating conditions such as cell temperature, humidity at each electrode, and stoichiometry. Their work focused on numerical simulation of the effects of operating conditions, especially cathode humidity, with simple microparallel flow channels and showed that the maximum power density could be obtained under conditions of 60% humidity and with a moderately high concentration of oxygen while maintaining high ion conductivity at a membrane. Eom et al. (2011) used radiofrequency identification tags to propose an improved Kalman filter method to reduce noise and obtain correct data because the system architecture is simple and can be adjusted by the neural network, leading to more accurate data obtained with the smart radiofrequency identification tags. Tang, Wang, Wang, and Li (2008) presented a non-invasive glucose measurement system that was based on the method of metabolic heat conformation; it consists of three temperature sensors, two humidity sensors, an infrared sensor, and an optical measurement device. The results of their experiments show that the glucose level can be deduced from the quantity of heat dissipation, blood flow rate of local tissue, and degree of blood oxygen saturation.

The impacts of time, temperature, and oxygen (O_2) concentration and flow are well documented in the efficient operation of CPAP devices. For example, Iftikhar et al. (2016) synthesized evidence from available studies on the relative efficacies of CPAP, mandibular advancement devices, supervised aerobic exercise training, and dietary weight loss in patients with obstructive sleep apnoea (OSA). The study found that CPAP decreased the apnoea–hypopnoea index. The experiment conclusions demonstrated that CPAP is the most efficacious means for complete resolution of sleep apnoea and in improving indices of O_2 saturation during sleep. In a similar fashion, Andrade et al. (2016) confirmed that CPAP is the gold standard treatment for OSA. Although CPAP was originally conceived to be applied through a nasal interface, the study of Andrade et al. was designed to determine the acute effects of changing the nasal CPAP route to an oronasal route. The authors found that, in patients with OSA, the oronasal route may compromise upper airway patency during sleep and thus CPAP effectiveness in treating OSA. They found that, compared with stable breathing through the nasal route, there were significant and progressive reductions in the distances between the epiglottis and tongue base and the retroglossal area when CPAP was delivered by oronasal and oral routes, respectively.

Andrade et al. (2016) indicated that CPAP delivered through the oronasal route may compromise the effectiveness of CPAP in treating OSA. Hewidy, Suliman, El Hefnawy, and Hassan (2016) provided evidence that non-invasive CPAP ventilation may improve post-operative oxygenation and lung function and reduce post-operative complications in morbidly obese patients undergoing sleeve gastrectomy. The authors evaluated the effect of immediate post-operative CPAP therapy after sleeve gastrectomy. The results showed that, in terms of both oxygen tension and saturation, the use of immediate CPAP after sleeve gastrectomy in morbidly obese patients is effective in improving oxygenation and spirometric values, reducing atelectasis, and decreasing post-operative pulmonary complications.

3.1 | Previous engineering design methodologies

Fuzzy logic has many business applications, and it has embraced many methods. For example, a novel method was proposed to mine association rules for classification problems, namely, axiomatic fuzzy set association rules for classification realized in the framework of the AFS theory (H. Wang, Liu, Pedrycz, & Zhu, 2011). Other papers have proposed a heuristic method for a resource-constrained project-scheduling problem with fuzzy activity times. This method was based on a priority rule for a parallel schedule generation scheme (Bhaskar, Pal, & Pal, 2010). Kao and Lin (2011) proposed that qualitative data should be viewed as fuzzy numbers and used data envelopment analysis multipliers associated with decision-making units, evaluating them to construct membership functions. Cluster analyses are sets of heuristic algorithms, and the term *cluster analysis* is a generic name for a variety of procedures that can be used to group data into natural sets (Hall, 1992). The factor analytic method is an algorithm approach method that forms a correlation matrix of similarities among cases. Classical factor analysis is then performed on the $N \times N$ matrix, and data are assigned to clusters on the basis of their factor loadings (Skinner, 1979). Fuzzy clustering has been applied to many

decision-making problems, from auditing to financial management to strategic portfolio management, and it has also been applied to multiobjective decision making (Ammar, Wright, & Selden, 2000; Bertram Tan & Hsieh, 2005; Yager, 1981).

Multisensor data fusion has many applications. For example, the output capability of a ball mill pulverizing system mainly represents the efficiency of the system. To measure output capability, a novel feature extraction method based on multisensor data fusion was proposed and an independent component analysis algorithm (FastICA) implemented to extract independent components from the field data, which included six sensor measurements (J. Wang & Liang, 2008). Multisensor data fusion methods for Gaussian noise have been widely reported, whereas fusion approaches for non-Gaussian noise are rare in the literature. However, four statistical fusion methods have been presented, for a mixture of Gaussian noise. These four methods are the minimum variance approach, the maximum kurtosis approach, the minimum kurtosis approach, and the minimum mean absolute error approach (Niu & Zhu, 2009). Data fusion algorithms have a wide range of applications in some fields, and there are also increasing sensor numbers in multisensor target tracking systems, data fusion algorithms using the conventional Kalman filter; however, the latter have problems such as heavy computational burden and poor robustness (Zhang & Wang, 2010). A critical aspect in designing a fuzzy logic Kalman filter is to make it robust to off-nominal behaviour caused by both degradation and anomalies (Kobayashi, Simon, & Litt, 2005). Following this method, fuzzy rules can replace mathematical rules, and decisions can be made more easily about how to use multisensor data fusion for optimal performance, given the outputs of the sensors (Klein, 2004).

3.2 | Nearest neighbour

Qi, Hu, and Peng (2012) stated that an adaptation phase is crucial for a good and reasonable case-based design process, which is responsible for finding a solution to solve a new problem in the principle of k-nearest neighbour (KNN). Their paper presented a new adaptation method for a solution featuring values of retrieved cases that could be adapted to our CPAP dataset. H. Chen et al. (2013) presented an effective and efficient diagnosis system using fuzzy KNN for the diagnosis of Parkinson's disease. The proposed fuzzy KNN-based system was compared with approaches based on support vector machines. García-Pedrajas and Ortiz-Boyer (2009) stated that the KNN classifier is one of the most widely used methods of classification for several interesting reasons, such as good generalization and easy implementation. Although it is simple, it is usually able to match and even surpass more sophisticated and complex methods to accurately classify difficult instances. This is one of the reasons why we chose to use the nearest neighbour (NN) method to investigate our CPAP datasets. Govindarajan and Chandrasekaran (2010) utilized text data mining as a process of exploratory data analysis. In a similar manner, we utilized factor analysis to help classify data into predefined groups or classes, such as temperature, oxygen concentration, and flow variables. This approach is often referred to as *supervised learning* because the classes are determined before the data and complements are examined. This segment of our analysis supports our unsupervised learning discipline, which was used in the clustering component of our algorithm. The paper described the proposed KNN classifier, which tested the feasibility of performing comparative cross-validation. The benefits of the proposed approach were demonstrated using data mining problems, similar to our study. Aci, Inan, and Avci (2010) created a hybrid method using five machine learning datasets: iris, breast cancer, glass, yeast, and wine. In our study, we also propose a hybrid approach that can be used with multiple CPAP databases. D. Li, Gu, and Zhang (2010) acknowledged that partially missing datasets are a prevalent problem in clustering analysis. In their paper, missing attributes were represented as intervals, and a novel algorithm for incomplete data based on NN intervals was proposed. In regard to future issues, our study could easily adapt this approach to handle missing data. C. Lee, Lin, Chen, and Kuo (2011) recently investigated the use of microarray technology to study gene expression in cancer diagnosis. In the past, researchers had used parametric statistical methods to discover significant genes. However, microarray data often do not follow some of the assumptions of parametric statistical methods, and Type I errors may be exaggerated. C. Lee et al. established a gene selection method devoid of assumption restrictions to reduce the dimensions of the dataset and to ensure that all test samples could be correctly classified. We faced a similar problem in our study when we attempted to correctly classify the various variables used to measure our oxygen concentration outcomes. S. Jiang, Pang, Wu, and Kuang (2012) recognized that text categorization is a significant tool for managing and organizing surging text data. Many text categorization algorithms have been explored, including KNN, naïve Bayes, and support vector machines. S. Jiang et al. (2012) proposed an improved KNN algorithm for text categorization that builds the classification model by combining a constrained one-pass clustering algorithm and KNN text categorization. The classification model constructed by the proposed algorithm can be updated incrementally and has great scalability for many real-word applications, such as text mining our CPAP datasets. Castillo, Melin, Ramírez, and Soria (2012) described a hybrid intelligent system for the classification of cardiac arrhythmias. The hybrid approach was tested with electrocardiogram records from the MIT-BIH Arrhythmia Database. The samples considered for classification contained four types of arrhythmias. The signals of the arrhythmias were segmented and transformed to improve the classification results. Three methods of classification were used to combine the outputs of the individual classifiers, and a very high classification rate of 98% was achieved. This approach could be useful for decision making in our study.

Artificial neural networks (ANNs) were created to mimic some of the phenomena observed in biology. The biological metaphor for ANNs is the human brain. An ANN consists of different sets of neurons or nodes and the connections between one set of neurons and another. Each connection between two nodes in different sets is assigned a weight that shows the strength of the connection. Connections with positive weights are called *excitatory connections*, and connections with negative weights are called *inhibitory connections* (Jain & Dubes, 1988; Rumelhart, Hinton, & William, 1986; Weiss & Kapouleas, 1989). Figure 1 shows a three-layer ANN.

The number of hidden layer neurons chosen was twice the number of data inputs, a commonly used heuristic (Bhattacharyya & Pendharkar, 1998).

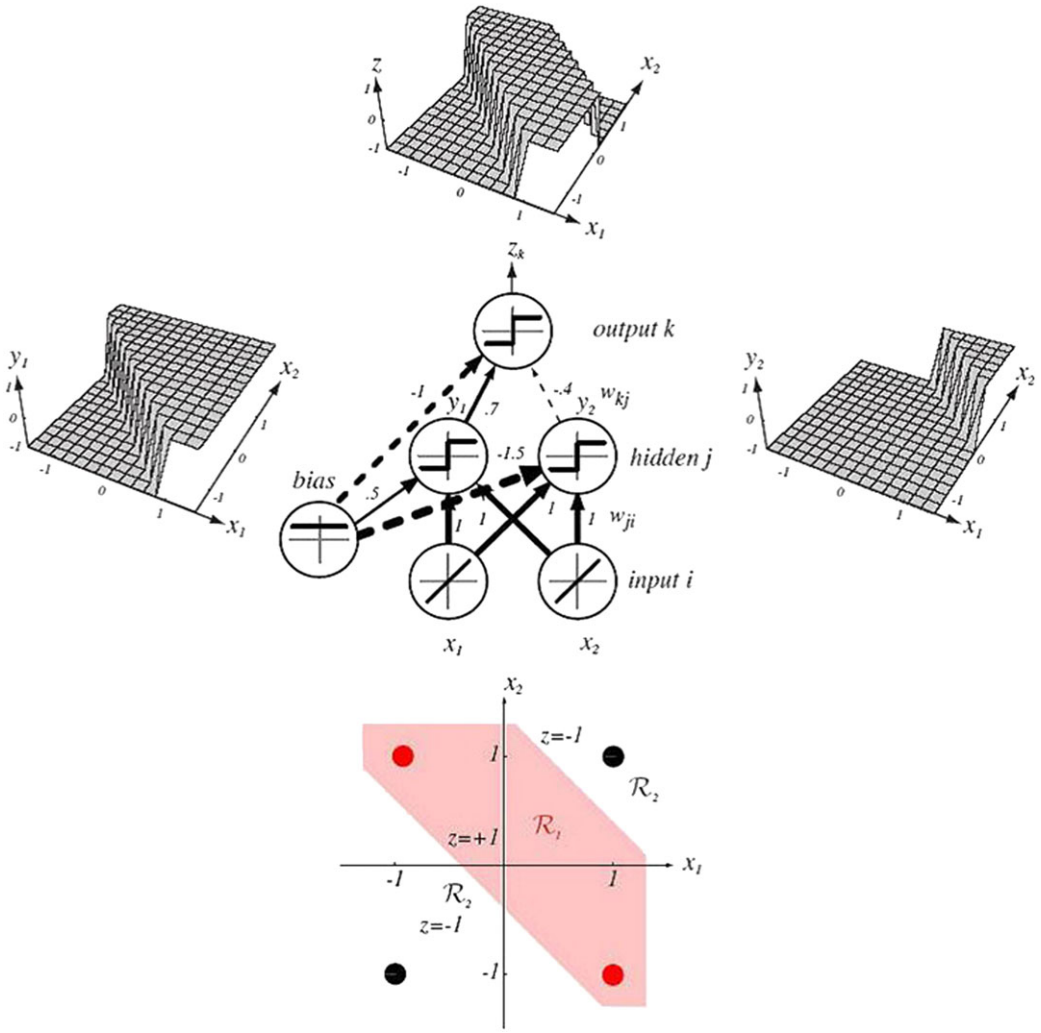

FIGURE 1 A three-layer artificial neural network

3.3 | Present Markov–Kalman viscosity engineering design methodology

Markov decision processes with a countable state space have long been common in the literature and may be applied to compute an optimal policy and average cost optimality. Kalman filtering is a forecasting technique that can serve as a building block for the model based on a linear space state (Aviv & Federgruen, 1999; Fleming, 1966; Soner, 1993). To improve CPAP viscosity, we first present a partially observable Markov decision process to forecast future oxygen demand. I then estimate the actual state of the system. Let $\{X_t\}$ be a finite, state-of-the-system, n-dimensional vector process. This vector may consist of actual demand and early demand indicators. This state vector can evolve accordingly:

$$\text{Dynamics of state space:} X_t = F X_{t-1} + V_t, \tag{1}$$

with an $n \times n$ matrix and F being a known time invariant. The white noise process is represented by the vectors $\{V_t \in \mathbf{R}^n: t \geq 1\}$. Each random vector V_t has a multivariate normal distribution with mean $\mathbf{0}_{n \times 1}$ and covariance matrix $\sum_V$. Assume that the state vector X_t is partially or fully observed by the decision maker. Only the vector is observed during time period t, where H is a known $m \times n$ matrix and the observation equation is

$$\Psi_t = H_t \varepsilon \mathbf{R}^m. \tag{2}$$

If Ψ_t is the decision maker's collected information during time t and D_t represents the realized demand during period t, then the demand can be considered to be a linear function and deterministic of the state vector and the demand equation is

$$D_t = \mu + R\Psi_t, \tag{3}$$

where R has known parameters as a $1 \times m$ vector and the known scalar is μ. To estimate the actual state of the system, I utilize the minimum mean square errors of the state X_t, a history of observations $\{\Psi_{t-1}, \Psi_{t-2}, \ldots, \Psi_1\}$, and estimate by $X\hat{}_t = E[X_t \mid \Psi_{t-1}, \Psi_{t-2}, \ldots, \Psi_1]$. In addition, let $\grave{U}_t^X = E[(X_t - X\hat{}_t)(X_t - X\hat{}_t)^t]$ be the error covariance.

The fuzzy Kalman filter approach is adapted to compute the values of $X\hat{}_t$ and $\grave{U}_t^X$ and to reduce the time necessary to perform complex matrix manipulations to control higher order systems such as in this CPAP model. Moreover, the fuzzy Kalman filter approach can capture the non-linearity of operation under the influence of anomalies. For instance, when a CPAP experiences component faults, the control system adjusts the actuator positions on the basis of the sensor feedback measurements to meet its objective (e.g., to maintain supply chain speed at the commanded value). As a result of this control adjustment, in addition to component faults, the CPAP moves to a new operating condition that may be a significant deviation from the nominal condition. Piecewise linear Kalman filters, designed along the operating line of the nominal condition, do not capture such off-nominal behaviour of a CPAP because of closed-loop control effects in the presence of anomalies.

The Kalman filter is in effect a set of recursive equations used to regenerate estimates of the state system at the beginning of each period. If one assumes an initial state vector estimate of $X\hat{}_1$ and an initial error covariance matrix of $\grave{U}_1^X$, then every beginning time period t has an estimate $X\hat{}_t$ produced by the following:

$$X\hat{}_t = F\,X\hat{}_{t-1} + FK_{t-1}(\Psi_{t-1} - H\,X\hat{}_{t-1}). \tag{4}$$

Furthermore, the associated error covariance matrix is computed as

$$\grave{U}^x{}_t = F\,\grave{U}^x{}_{t-1}F^{\mathrm{T}} - FK_{t-1}\,H\,\grave{U}^x{}_{t-1}\,F^{\mathrm{T}} + \sum_V, \tag{5}$$

where $K_{t-1} = \grave{U}^x{}_{t-1}H^{\mathrm{T}}(H\grave{U}^x{}_{t-1}\,H^{\mathrm{T}})^{-1}$ is an $n \times m$ Kalman gain matrix.

The J-link, processor, concentrator, thermistor, and the piezotransducers are the instrument used in the project. The J-link is also used for powering up the microprocessor; after this, the J-link sends an activation signal to the Processor. Once the J-link gets a signal from the processor then initiates the oxygen concentrator. When the oxygen concentrator is initiated, its main function is to start pumping oxygen into the thermistor; else, it displays an error message, and the piezotransducers trigger a sonic wave when the oxygen passes through the thermistor, and it also displays the output. If there are no sonic waves triggered, an error message pops up.

Decision trees are used when there is complex branching. It consists of nodes and branches. Trees are also used to describe the consequences of a decision. It involves structured decision process, and trees are used to keep a string of decision in a particular sequence. Decision trees help in identifying the orders and timing of an event. Decision trees are easily understood by the user and help in executing the actions according to their timings. Structured English is used when the communication with the end users is very important. It is an effective method to avoid impossible situations, redundancies, and contradictions. Decision tree provides a framework to calculate the values of the outcomes and the probability of achieving them. This helps in achieving best results with the available information. Here we have outlined bullet points to prioritize the events and help in constructing a structured and sequential decision tree method for the execution of the events.

- J-link—The J-link microcontroller is switched on through a power source; this also powers up the microprocessor. The user gets an alert on the laptop.
- Laptop—Laptop displays all the required attributes that the user needs. It is used to monitor the process.
- Processor—The signal received from the J-link microcontroller initiates the processor, and this in turn initiates the oxygen concentrator.
- Oxygen concentrator—The oxygen concentrator then starts generating oxygen and is sent to the thermistor. If the oxygen concentrator is not generating any oxygen, then an error message pops up for the user to debug.
- Thermistor—This sensor checks the temperature of the oxygen, and if the temperature is in the required range, then it is forwarded to the piezotransducer, and if the required temperature is not reached, then the thermistor adjusts the oxygen temperature to the requirement.
- Piezotransducer—Once the oxygen passes through the thermistor, the piezotransducer triggers the sonic wave; the output is displayed. An error message is popped up if no sonic waves are triggered.

The data start when the user switches on the system. The microprocessor is then sent the signals to measure the temperature of the tube and then to initialize the standard variables for calculating the oxygen concentration and the flow rate. Then, the thermistor is used to calculate the temperature, and then the piezotransducers are used to send a single sonic wave through the concentrator to measure the time it takes for the sound to pass through the tube. All these data are captured by the microprocessor and then are used to calculate the concentration and the flow rate of oxygen through the tube. These data are then stored in the database, which can then be used to measure the quality and the performance of the concentrator, where the data stores are time taken, temperature, and user log.

The processes are the sending of the start signal to the microprocessor, the feedback to the database, and the input data to the thermistor and the transducers. The entities of the system are the user, the thermistor, the microprocessor, the database, and the piezotransducers. The preliminary engineering design and workflow are illustrated in Figure 2. The use case scenarios and events are shown in Figures 3 and 4.

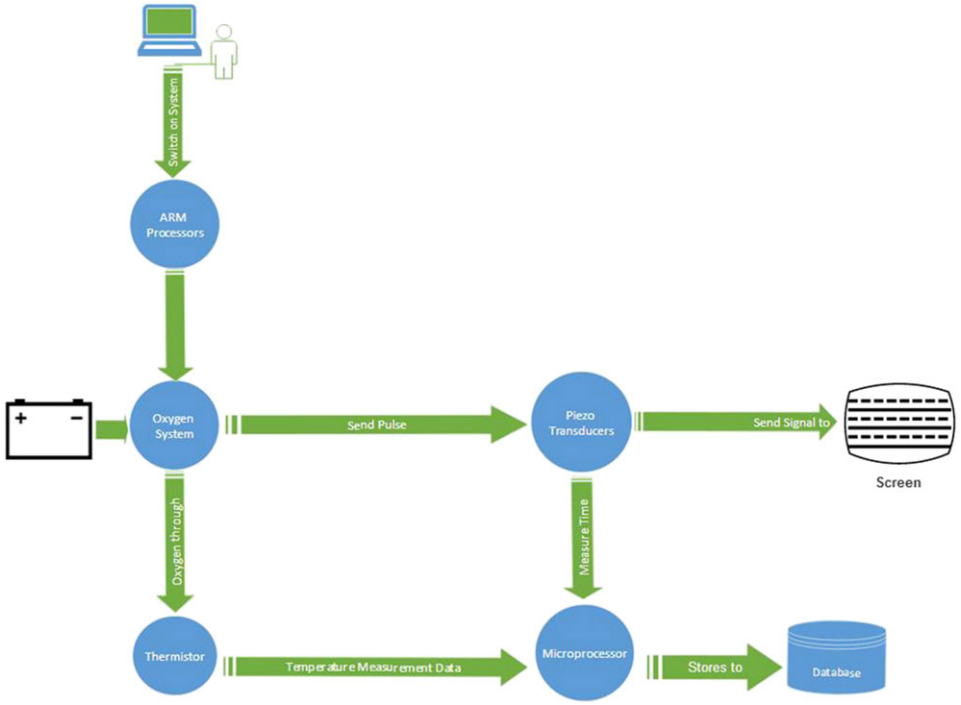

FIGURE 2 Preliminary engineering design and workflow diagram

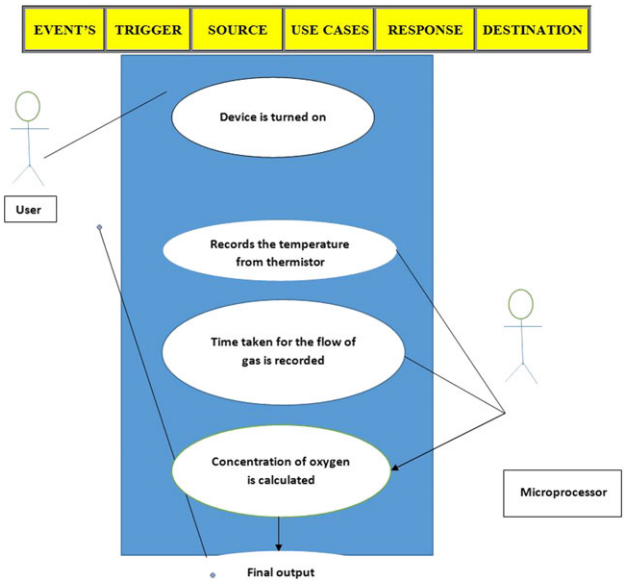

FIGURE 3 Use case diagram

4 | ANALYSIS AND PARTITION OF THE CPAP SYSTEM

Given the aforementioned applications of multisensor data fusion, it is likely that various methodologies, including fuzzy control, can be applied to CPAP air delivery, for which rules are established for such continuous variables as oxygen concentration, air flow, air temperature, average delivery time, and time with and against pressure (T_{with} and $T_{against}$). Factor analysis places these six variables into three clusters (i.e., time and temperature, flow, and oxygen concentration): tempfluke, T_{with} and $T_{against}$, and tempsensor load on Factor 1 (.999, −.973, −.966, and .999, respectively) and flow loads on Factor 2 (1.000) and O_2 loads on Factor 3 (.999). These results are seen in Table 1.

The complete set of production rules needed to associate new data with risk is shown in Table 2.

The input and output membership functions are illustrated in Figures 5, 6, and 7. Figure 8 shows the nine rules generated. Figure 9 shows the surface map from the inputs of flow and temperature along with the oxygen concentration output.

Oxygen concentrator device is turned ON	Switch	Cables and Voltage	Device is turned ON	Device is ON	Device
Oxygen flow is generated	Device	Statistics from the Monitor	Generate Oxygen flow	Generates oxygen flow with sonic waves and transmitted gas	Receiver
Trigger sonic waves	Driver	Time intervals between trigger and pulse in the device	Generates sonic waves	Sonic waves are triggered with respective to the time intervals	Piezo Transducer
Measure time taken by sonic wave	Piezo Transducer	Pulse count from Processor	Measures time taken by sonic wave between the intervals	Send the measured time	Microprocessor
Tube temperature recorded.	Receiver	Processor collected pulse count	Temperature values are noted by Thermistor	Store the pulse count measured by sonic waves	Thermistor
Calculate Oxygen Concentration and Flow rate	Microprocessor	Gas temperature received from Thermistor	Uses Stored formulas and measures time taken by the clock pulse, Temperature and Constant Values.	Sends the data to storage device	Secondary storage
Display the Output	Microprocessor	Collect data from Secondary Storage	Calculated result of Percentage and Volume	Displays the Output on Monitor	Monitor

FIGURE 4 Events

TABLE 1 Factor analysis

Rotated component matrix[a]			
	Component		
	1	2	3
Flow	0.003	1.000	0.000
Tempfluke	0.999	0.011	0.029
T_{with}	−0.973	−0.197	0.110
$T_{against}$	−0.966	0.232	0.109
Tempsensor	0.999	0.012	0.029
O_2	−0.045	0.001	0.999

Note. Extraction method: Principal component analysis.

Rotation method: Varimax with Kaiser normalization.

[a]Rotation converged in three iterations.

5 | RESULTS

To add internal and external validity to our data fusion study, we decided to adopt a multiple methodology, longitudinal approach to our CPAP sensor experiments, as this method is common in the literature (Aziz, 2014; Banerjee & Das, 2012; Chien, Hsu, Morrison, & Dou, 2016; Elfaki, 2016;

TABLE 2 Fuzzy association memory rules for degree of risky continuous positive airway pressure health

Temperature (°C)	Flow rate (L/min)		
	Low	Medium	High
Low	Low	Low	Medium
Medium	Low	Medium	High
High	Medium	High	High

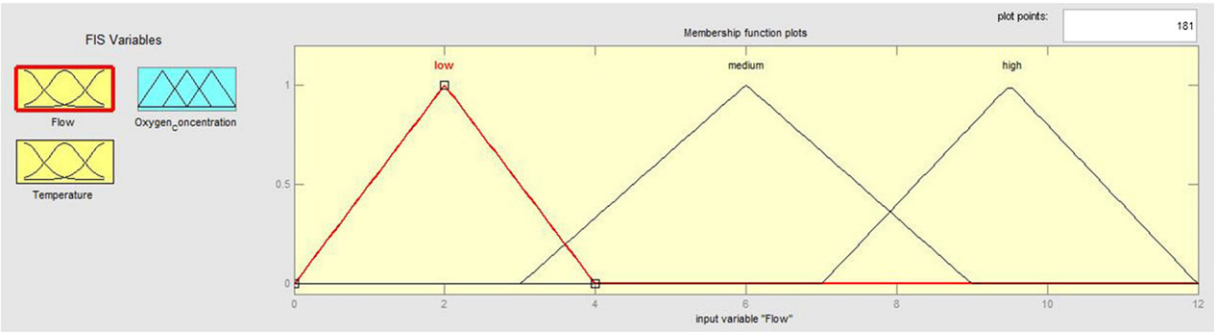

FIGURE 5 Flow fuzzy membership

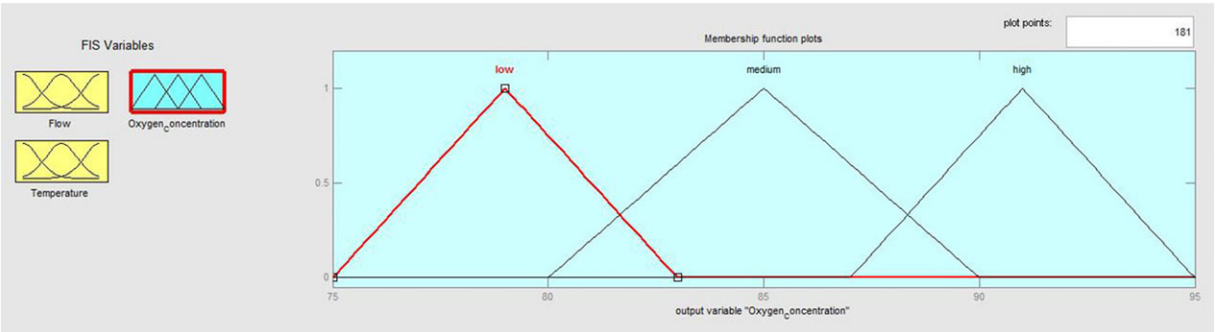

FIGURE 6 Oxygen fuzzy membership

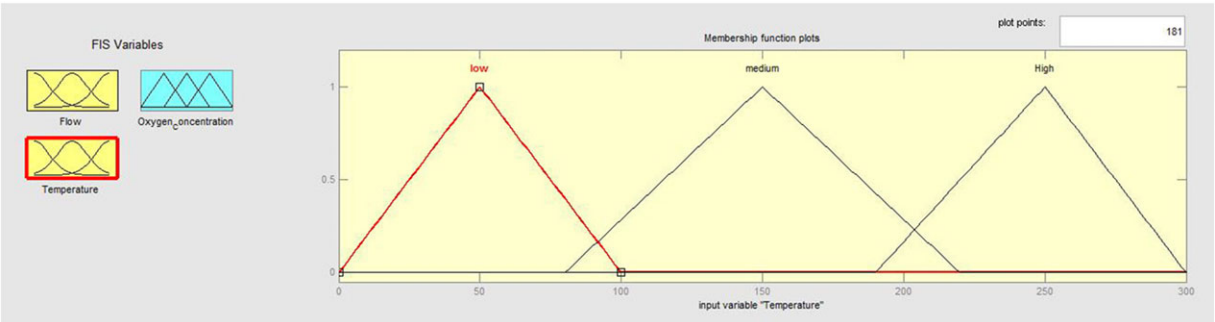

FIGURE 7 Temperature fuzzy membership

Zhu, Leung, & He, 2013). Although this original dataset consisted of a sample of only 40 data points, it did give us some preliminary insights to solving our quality control issues. Table 3 demonstrates the high initial correlations between flow, temperature, and oxygen concentration. These results show that our data follow the accepted gas laws of Guy Lussac, Boyle, and Charles and add external validity and generalizability to our study results.

1. If (Flow is low) and (Temperature is low) then (Oxygen_Concentration is low) (1)
2. If (Flow is medium) and (Temperature is medium) then (Oxygen_Concentration is medium) (1)
3. If (Flow is high) and (Temperature is High) then (Oxygen_Concentration is high) (1)
4. If (Flow is low) and (Temperature is medium) then (Oxygen_Concentration is low) (1)
5. If (Flow is low) and (Temperature is High) then (Oxygen_Concentration is low) (1)
6. If (Flow is medium) and (Temperature is low) then (Oxygen_Concentration is low) (1)
7. If (Flow is medium) and (Temperature is High) then (Oxygen_Concentration is medium) (1)
8. If (Flow is high) and (Temperature is low) then (Oxygen_Concentration is medium) (1)
9. If (Flow is high) and (Temperature is medium) then (Oxygen_Concentration is high) (1)

FIGURE 8 Fuzzy rules for oxygen concentration, flow, and temperature

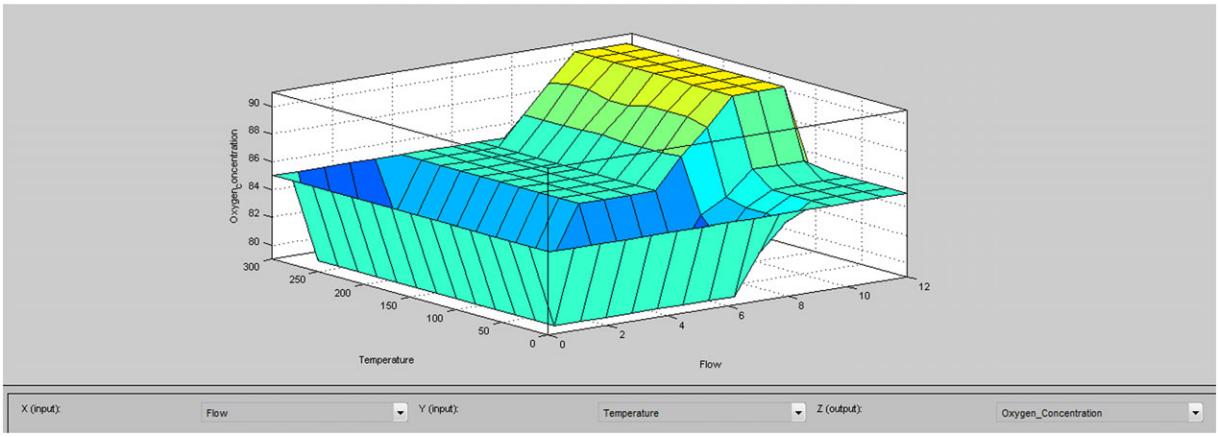

FIGURE 9 Surface map of flow, temperature, and oxygen concentration

TABLE 3 Correlations

	O_2	Flow	Tempfluke	T_{with}	$T_{against}$	Tempsensor	
O_2	Pearson correlation	1	.000	−.016	.153	.152	−.016
	Sig. (two tailed)		.998	.923	.345	.349	.923
	N	40	40	40	40	40	40
Flow	Pearson correlation	.000	1	.014	−.200	.228	.015
	Sig. (two tailed)	.998		.933	.216	.156	.927
	N	40	40	40	40	40	40
Tempfluke	Pearson correlation	−.016	.014	1	−.970**	−.958**	1.000**
	Sig. (two tailed)	.923	.933		.000	.000	.000
	N	40	40	40	40	40	40
T_{with}	Pearson correlation	.153	−.200	−.970**	1	.907**	−.970**
	Sig. (two tailed)	.345	.216	.000		.000	.000
	N	40	40	40	40	40	40
Timeagainst	Pearson correlation	.152	.228	−.958**	.907**	1	−.957**
	Sig. (two tailed)	.349	.156	.000	.000		.000
	N	40	40	40	40	40	40
Tempsensor	Pearson correlation	−.016	.015	1.000**	−.970**	−.957**	1
	Sig. (two tailed)	.923	.927	.000	.000	.000	
	N	40	40	40	40	40	40

**Correlation is significant at the .01 level (two tailed).

The temperature of the sensor and the temperature of the fluke are very highly correlated at 1.000. As the temperature of the fluke rises, there is a decrease in T_{with} (−.970) and $T_{against}$ (−.958) at the .01 level of significance. In a similar manner, as the temperature of the sensor rises, there is a decrease in T_{with} (−.970) and $T_{against}$ (−.957) at the .01 level of significance. Charles's law states that the volume is directly proportional to its

absolute temperature: $V1/T1 = V2/T2$. Also, Guy Lussac states that $P1/T1 = P2/T2$. Boyle's law states that the volume of a gas at constant temperature is inversely proportional to the pressure to which it is subjected: $P1/P2 = V2\ V1$. In our adaptation, the effect of increasing pressure will lead to decreasing the volume of the O_2. Increasing the temperature of a reacting system in equilibrium will increase the velocities of the reactions in both directions. When any reaction proceeds in one direction, then heat is either evolved or absorbed.

Table 4 demonstrates the descriptive statistics associated with this exploratory initial dataset.

TABLE 4 Statistics

		O_2	Flow	Tempfluke	T_{with}	$T_{against}$	Tempsensor
N	Valid	40	40	40	40	40	40
	Missing	2	2	2	2	2	2
Mean		87.000000	4.278975	24.932500	0.000224360842500	0.000226678965000	24.5422175
Standard error of mean		0.8227534	0.6322335	2.7918181	0.000000689640013	0.000000706954024	2.77328614
Median		87.000000	3.079000	20.400000	0.000225584100000	0.000227647550000	19.8999500
Mode		80.0000[a]	5.2000	20.4000[a]	0.0002166611000[a]	0.00021848780000[a]	49.70000
Standard deviation		5.2035491	3.9985954	17.6570083	0.000004361666416	0.000004471169837	17.53980160
Variance		27.077	15.989	311.770	0.000	0.000	307.645
Skewness		−0.271	0.614	0.513	−0.452	−0.500	0.520
Standard error of skewness		0.374	0.374	0.374	0.374	0.374	0.374
Kurtosis		−1.422	−1.237	−1.317	−1.180	−1.070	−1.315
Standard error of kurtosis		0.733	0.733	0.733	0.733	0.733	0.733
Range		13.0000	10.4190	44.5000	0.0000138497000	0.00001479590000	44.30000
Minimum		80.0000	0.4710	5.7000	0.0002166611000	0.00021848780000	5.40000
Maximum		93.0000	10.8900	50.2000	0.0002305108000	0.00023328370000	49.70000
Sum		3,480.0000	171.1590	997.3000	0.0089744337000	0.00906715860000	981.68870

[a]Multiple modes exist. The smallest value is shown.

TABLE 5 Model summary

Model	*R*	R^2	Adjusted R^2	Standard error of the estimate
1	.892[a]	.796	.773	2.4788625

[a]Predictors: (Constant), tempsensor, flow, $T_{against}$, T_{with}.

TABLE 6 Analysis of variance[a]

Model		Sum of squares	*df*	Mean square	*F*	Sig.
1	Regression	840.933	4	210.233	34.213	.000[b]
	Residual	215.067	35	6.145		
	Total	1,056.000	39			

[a]Dependent variable: O_2.

[b]Predictors: (Constant), tempsensor, flow, $T_{against}$, T_{with}.

TABLE 7 Coefficients[a]

Model		Unstandardized coefficients		Standardized coefficients	*t*	Sig.
		B	Standard error	β		
1	(Constant)	−1,496.450	135.523		−11.042	.000
	Flow	0.255	0.910	0.196	0.280	.781
	T_{with}	4,459,169.434	1,963,135.486	3.738	2.271	.029
	$T_{against}$	2,388,060.889	1,907,372.294	2.052	1.252	.219
	Tempsensor	1.653	0.144	5.573	11.517	.000

[a]Dependent variable: O_2.

TABLE 8 Excluded variables[a]

Model		β In	*t*	Sig.	Partial correlation	Collinearity statistics (tolerance)
1	Tempfluke	−6.559[b]	−0.770	.447	−.131	8.113E−5

[a]Dependent variable: O_2.

[b]Predictors in the model: (Constant), tempsensor, flow, timeagainst, timewith.

TABLE 9 Correlations

		O_2	Flow	T_{with}	$T_{against}$	TempC	AVGtime	Δtime	TempKelvin
O_2	Pearson correlation	1	.040	.013	.029	−.012	.022	.038	−.012
	Sig.		.404	.782	.548	.811	.652	.428	.811
	N	430	430	430	430	430	430	430	430
Flow	Pearson correlation	.040	1	−.186**	.233**	−.065	.026	.993**	−.065
	Sig.	.404		.000	.000	.179	.585	.000	.179
	N	430	430	430	430	430	430	430	430
T_{with}	Pearson correlation	.013	−.186**	1	.911**	−.384**	.977**	−.157**	−.384**
	Sig.	.782	.000		.000	.000	.000	.001	.000
	N	430	430	430	430	430	430	430	430
$T_{against}$	Pearson correlation	.029	.233**	.911**	1	−.408**	.978**	.264**	−.408**
	Sig.	.548	.000	.000		.000	.000	.000	.000
	N	430	430	430	430	430	430	430	430
TempC	Pearson correlation	−.012	−.065	−.384**	−.408**	1	−.405**	−.080	1.000**
	Sig.	.811	.179	.000	.000		.000	.096	.000
	N	430	430	430	430	430	430	430	430
AVGtime	Pearson correlation	.022	.026	.977**	.978**	−.405**	1	.057	−.405**
	Sig.	.652	.585	.000	.000	.000		.235	.000
	N	430	430	430	430	430	430	430	430
Δtime	Pearson correlation	.038	.993**	−.157**	.264**	−.080	.057	1	−.080
	Sig.	.428	.000	.001	.000	.096	.235		.096
	N	430	430	430	430	430	430	430	430
TempKelvin	Pearson correlation	−.012	−.065	−.384**	−.408**	1.000**	−.405**	−.080	1
	Sig.	.811	.179	.000	.000	.000	.000	.096	
	N	430	430	430	430	430	430	430	430

**Correlation is significant at the .01 level (two tailed).

TABLE 10 Model summary

Model	*R*	R^2	Adjusted R^2	Standard error of the estimate
1	.993[a]	.986	.986	.401366

[a]Predictors: (Constant), TempKelvin, flow, T_{with}, $T_{against}$.

TABLE 11 Analysis of variance[a]

Model		Sum of squares	*df*	Mean square	*F*	Sig.
1	Regression	4,909.691	4	1,227.423	7,619.250	.000[b]
	Residual	68.465	425	0.161		
	Total	4,978.156	429			

[a]Dependent variable: O_2.

[b]Predictors: (Constant), TempKelvin, flow, T_{with}, $T_{against}$.

TABLE 12 Coefficients[a]

Model		Unstandardized coefficients		Standardized coefficients		
		B	Standard error	β	*t*	Sig.
1	(Constant)	4.981	1.401		3.555	.000
	Flow	0.002	0.004	0.003	0.508	.612
	T_{with}	−1,993,631.078	11,760.481	−2.342	−169.520	.000
	$T_{against}$	1,968,245.904	11,621.878	2.368	169.357	.000
	TempKelvin	0.001	0.001	0.003	0.499	.618

[a]Dependent variable: O_2.

TABLE 13 Rotated component matrix[a]

	Component		
	1	2	3
Flow	−0.063	0.994	−0.059
T_{with}	0.973	−0.138	−0.182
$T_{against}$	0.937	0.281	−0.206
TempC	−0.215	−0.022	0.976
AVGtime	0.977	0.076	−0.199
Δtime	−0.033	0.995	−0.068
TempKelvin	−0.215	−0.022	0.976
O_2	0.033	0.078	0.008

Note. Extraction method: Principal component analysis.
Rotation method: Varimax with Kaiser normalization.[a]
[a]Rotation converged in five iterations.

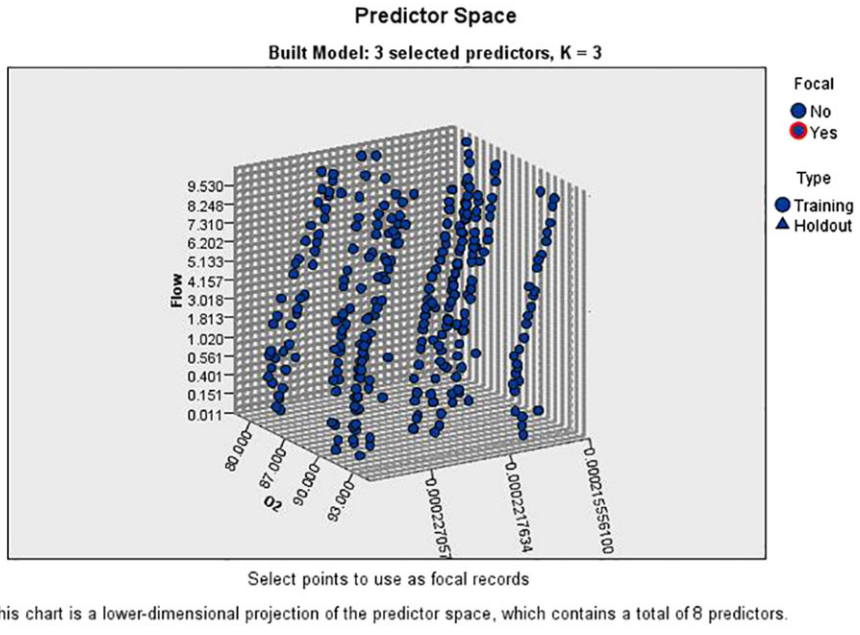

FIGURE 10 Relationship between flow, O_2, and time

All data appear to be normally distributed according to the kurtosis and skewness. Standard deviations are small for O_2 and flow and slightly larger for temperatures. Standard deviations for time are minute. The range of both the fluke and sensor are about 44°.

Table 5 illustrates that about 80% of the O_2 concentration is explained by the temperature of the sensor, flow, $T_{against}$, and T_{with}.

Table 6 indicates that the overall model is significant at the .000 level of significance and that temperature of the sensor, flow, $T_{against}$, and T_{with} will have an impact on oxygen concentration.

TABLE 14 Statistics

		O_2	Flow	T_{with}	$T_{against}$	TempC	AVGtime	Δtime	TempKelvin
N	Valid	430	430	430	430	430	430	430	430
	Mis	0	0	0	0	0	0	0	0
Mean	87.13721	3.83580	0.0002234794030	0.0002256101304	34.36519	0.0002245	0.0000021	307.51	
Standard error of mean	0.237884	0.164275	0.0000001930140	0.0000001976425	0.982105	0.0000001	0.00000008	0.98210	
Median	90.00000	3.08000	0.0002231229500	0.0002255286000	34.60000	0.0002245	0.0000019	307.74	
Mode	90.000	0.122	0.000215556100[a]	0.000215562100[a]	49.910	0.000215[a]	−0.000000074400[a]	323.06	
Standard deviation	4.932860	3.406478	0.0000040024251	0.0000040984033	20.36536	0.0000039	0.0000017	20.365	
Variance	24.333	11.604	0.000	0.000	414.748	0.000	0.000	414.75	
Skewness	−0.578	0.511	−0.009	−0.123	4.511	−0.079	0.299	4.511	
Standard error of skewness	0.118	0.118	0.118	0.118	0.118	0.118	0.118	0.118	
Kurtosis	−1.316	−1.134	−1.123	−1.042	55.692	−1.181	−1.366	55.692	
Standard error of kurtosis	0.235	0.235	0.235	0.235	0.235	0.235	0.235	0.235	
Range	13.000	10.879	0.000015063100	0.000017721600	283.700	0.0000153	0.0000053	283.70	
Minimum	80.000	0.011	0.000215556100	0.000215562100	5.400	0.0002155	−0.00000007	278.55	
Maximum	93.000	10.890	0.000230619200	0.000233283700	289.100	0.0002309	0.0000053	562.25	
Sum	37,469.00	1,649.393	0.096096143300	0.097012356100	14,777.03	0.0965542	0.0009162	231.51	

[a]Multiple modes exist. The lowest value is shown.

Table 7 shows that the T_{with} (.029) and temperature of the sensor (.000) contribute the most to the O_2 concentration.

Table 8 gives an interesting insight in that the temperature of the fluke was excluded from the model because it correlated so highly with the temperature of the sensor. Therefore, it also contributes to the model at ($p \leq .000$). The successful insights of the preliminary data gave our study impetus to follow up on the encouraging initial exploratory results and to collect a larger and more powerful sample of 430 data points in a second more robust dataset.

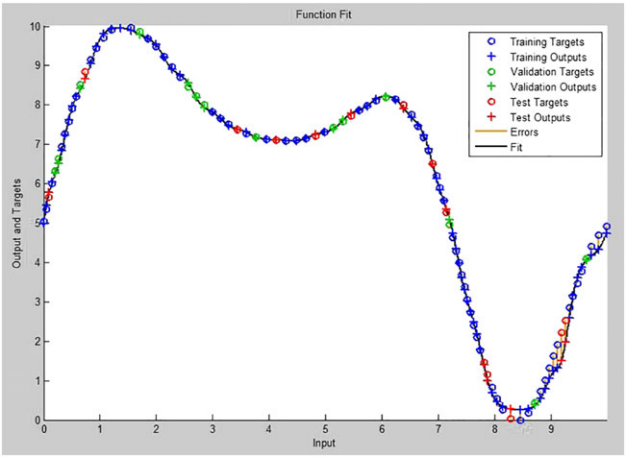

FIGURE 11 Artificial neural network fit

```
%CREATE_FIT_NET Creates and trains a fitting neural network.
%
%  NET = CREATE_FIT_NET(INPUTS,TARGETS) takes these arguments:
%    INPUTS - RxQ matrix of Q R-element input samples
%    TARGETS - SxQ matrix of Q S-element associated target samples
%  arranged as columns, and returns these results:
%    NET - The trained neural network
%
%  For example, to solve the Simple Fit dataset problem with this function:
%
%    load simplefit_dataset
%    net = create_fit_net(simplefitInputs,simplefitTargets);
%    simplefitOutputs = sim(net,simplefitInputs);
%
%  To reproduce the results you obtained in NFTOOL:
%
%    net = create_fit_net(simplefitInputs',simplefitTargets');

% Create Network
numHiddenNeurons = 20;  % Adjust as desired
net = newfit(inputs,targets,numHiddenNeurons);
net.divideParam.trainRatio = 70/100;  % Adjust as desired
net.divideParam.valRatio = 15/100;  % Adjust as desired
net.divideParam.testRatio = 15/100;  % Adjust as desired

% Train and Apply Network
[net,tr] = train(net,inputs,targets);
outputs = sim(net,inputs);

% Plot
plotperf(tr)
plotfit(net,inputs,targets)
```

FIGURE 12 Matlab mfile code

Our new dataset yields some new and interesting relationships between the variables. For example, Table 9 illustrates that flow is significant at the .01 level for T_{with}, $T_{against}$, and Δtime (−.186, .233, .993). T_{with} shows a significant relationship with all variables except oxygen concentration (.013). It is also interesting to note that flow is inversely related (−.186), as is temperature in degrees Celsius (−.384), Δtime (−.157), and temperature in Kelvin (−.384). $T_{against}$ seems to have a significant relationship with flow (.233) and an inverse relationship with temperature (−.408).

The R^2 as shown in Table 10 has improved from the exploratory dataset at 79.6% to 98.6% for our robust model. In other words, almost 99% of the variation in oxygen concentration is explained by variations in the flow, temperature, and time variables.

As illustrated in Table 11, our regression analysis remains significant in both datasets at p = .000. It is interesting to see that, whereas the oxygen concentration is not significantly correlated with any of the independent variables, the overall model is significant. This seems to imply that oxygen concentration is determined by the combined effects of flow, time, and temperature, as stated in our original research question.

Table 12 shows that T_{with} and $T_{against}$ are major contributors to oxygen concentration. T_{with} has a negative inverse relationship (β = −2.342) and $T_{against}$ has a positive relationship (2.368).

Table 13 gives the rotated component analysis and shows that the variables T_{with} (0.973), $T_{against}$ (0.937), and average time (0.977) all load on Component 1. Flow (0.994) and Δtime (0.995) load on Component 2. Finally, temperature in degrees Celsius and Kelvin both load on Component 3 (0.976). Oxygen concentration does not load on any of these factors, indicating that a combination of time, flow, and temperature is necessary to deliver the required O_2 to the CPAP device.

Figure 10 shows the NN predictor space and the relationships between flow, O_2, and time. This graphic reinforces our conclusions that the oxygen concentration is dependent on time and the flow rate, as indicated by the blue lines. The NN experiments had a total of 286 samples trained, with 144 holdouts and 1 excluded sample. The predictor space gave excellent results when time, temperature, and flow were used as predictors of oxygen concentration delivered by the CPAP. These experiments also showed that in a comparison of the actual and predicted NN, the

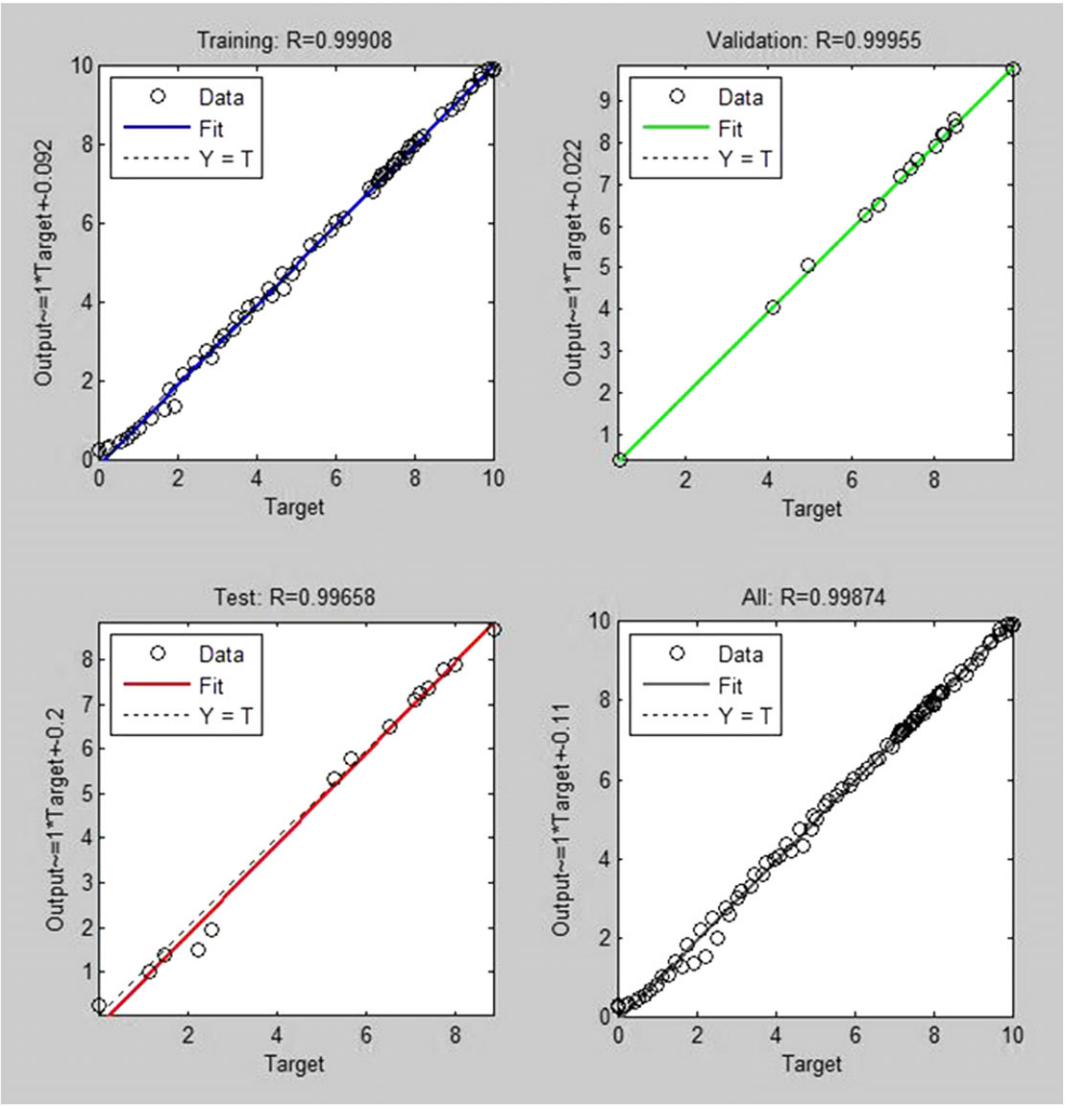

FIGURE 13 Plot regression

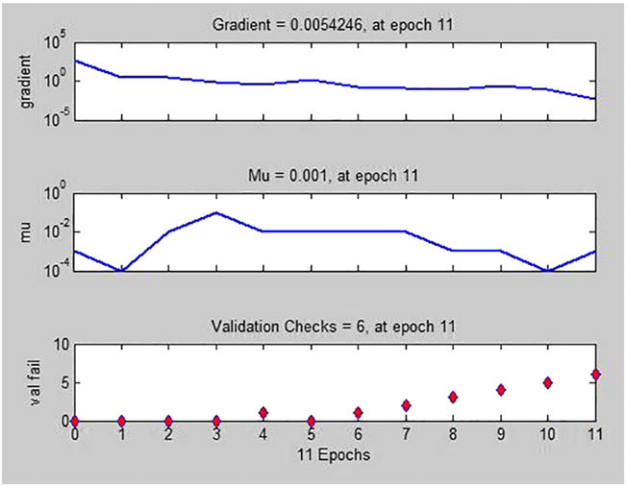

FIGURE 14 Training state

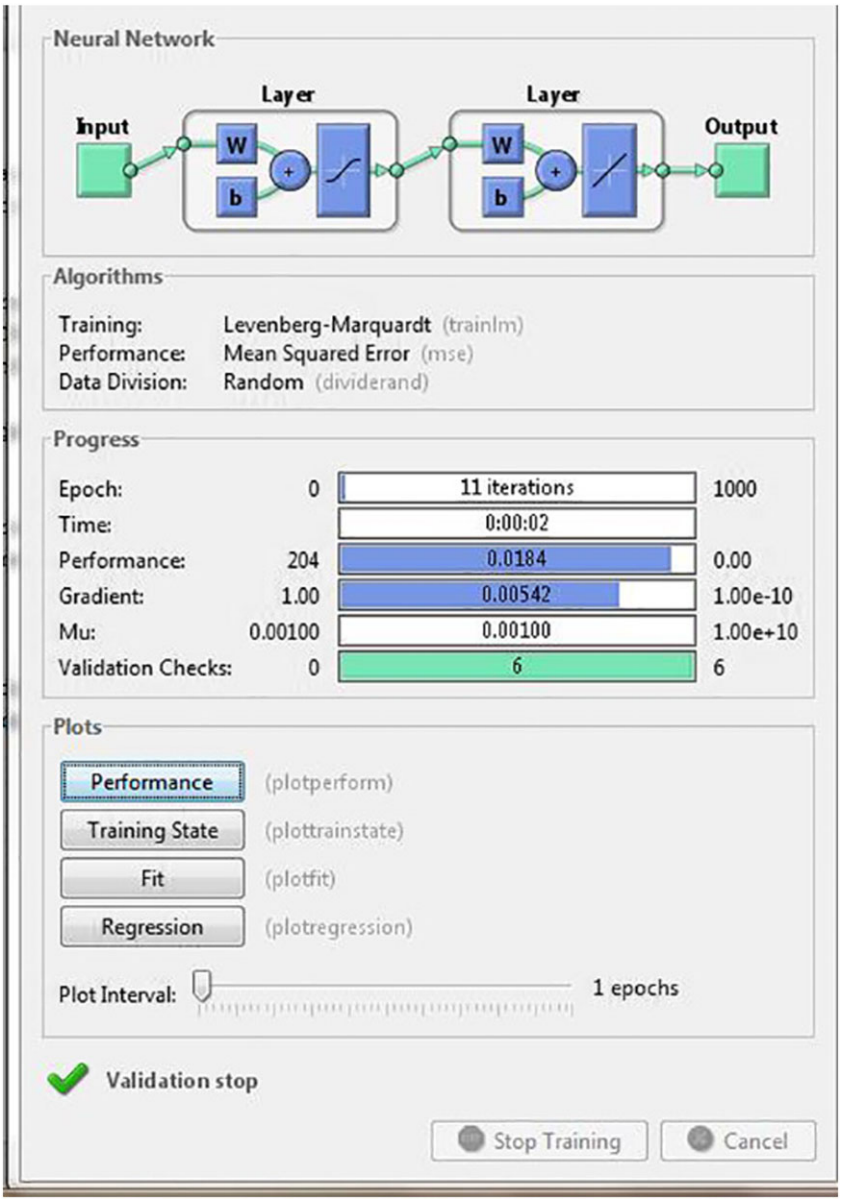

FIGURE 15 Artificial neural network training

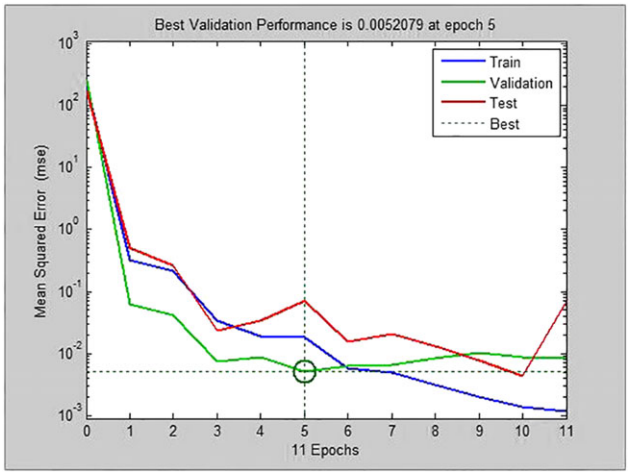

FIGURE 16 Artificial neural network validation

TABLE 15 Case processing summary

		N	%
Sample	Training	293	93.0
	Testing	22	7.0
Valid		315	100.0
Excluded		115	
Total		430	

TABLE 16 Network information

Input layer	**Factors**	**1** **2** **3** **4** **5** **6** **7**	**Flow** **T_{with}** **$T_{against}$** **TempC** **AVGtime** **Δtime** **TempKelvin**
	Number of units[a]	**1,450**	
Hidden layer(s)	Number of hidden layers	1	
	Number of units in Hidden Layer 1[a]	18	
	Activation function	Hyperbolic tangent	
Output layer	Dependent variables	1	O_2
	Number of units	1	
	Rescaling method for scale dependents	Standardized	
	Activation function	Identity	
	Error function	Sum of squares	

[a]Excluding the bias unit.

TABLE 17 Model summary

Training	**Sum of squares error** **Relative error** **Stopping rule used** **Training time**	**0.114** **0.001** **1 consecutive step(s) with no decrease in error[a]** **0:00:01.71**
Testing	Sum of squares error	0.007
	Relative error	0.000

Note. Dependent variable: O_2.

[a]Error computations are based on the testing sample.

means were very close, at 87.12% and 87.22% O_2 concentrations, respectively. These findings are further supported by a Pearson correlation of .954 and a Spearman rho of 0.943 between the two values, with p = .000 and a standard error of the mean of 1.54135. These NN results give further evidence that alternative methods such as fuzzy logic and ANN may provide additional insights into the relationships among items in our dataset and that these methods warrant consideration.

The descriptive statistics, shown in Table 14, are normally distributed and parametric. They show the importance of the η power that has been applied due to the larger sample size over the initial exploratory dataset.

5.1 | ANN model experiments

On the basis of the CPAP system data, we trained an overall neural net model. Each pattern consisted of the seven inputs of flow, T_{with}, $T_{against}$, TempC, AVGtime, Δtime, and TempKelvin. The output was the O_2 concentration in percent. All inputs and outputs had variation and were not constant. Figure 11 shows the functional fit between the input variables and the outputs and targets.

Figure 12 shows the C++ Matlab mfile software code used to run the ANN.

The best validation performance, function fit, and regression values, comparing the real and predicted ANN values of the CPAP system efficiencies, are shown in Figure 11. Note that the predicted values were close to the real values, and therefore, the neural net model developed had acceptable accuracy. Also note that this model had two more variables than the previously proposed linear regression model. The overall R value was .99874, the test R was .99658, the training R was .9998, and the validation R was .99958, as shown in Figure 13.

Figure 14 shows the gradient of 0.0064246 at Epoch 11, a μ of 0.001 at Epoch 11, and validation failure checks of 6 at Epoch 11.

Figure 15 shows the ANN training algorithms, training, and plots. The quality of the results depended on the number of hidden nodes.

The mean square error for the testing was approximately $10^{-1.3}$, for training was approximately $10^{-1.8}$, and for validation was approximately $10^{-2.3}$, as seen in Figure 16. The best validation performance is 0.0052079 at Epoch 5 of the 11 epochs.

Table 15 illustrates that of the 430 data points, 293 samples were presented to the network during training, and the network was adjusted according to its error. Finally, 22 samples were used for testing and had no effect on training; these provided an independent measure of network performance during and after training. Moreover, 115 samples were excluded and used to validate or measure the network generalization and to halt training when generalization stopped improving.

We chose 18 as the number of units in the hidden layer, as this was the smallest number of hidden neurons with acceptable least square errors over the training and test regions. These results are presented in Table 16.

Table 17 provides the model summary for the ANN. In the training, the sum of squares error was 0.114 and the relative error was 0.001. For the testing, the sum of squares error was 0.007 and the relative error was 0.000. These values are well within acceptable ranges.

6 | CONCLUSIONS

In the original dataset, we did find that there was random noise on the received signal. Thus, the data that we collected were exploratory. We put an amplifier circuit on the received signal to remove the noise, and this modification gave very repeatable results. We learned that we need to read the transit time within ±50 ns for ±1% oxygen. In our assumptions for measuring oxygen, we concluded that the time advance of the sound wave with flow is equivalent to the time lag of the sound wave against flow. So the average of with and against gives an equivalent time travel at 0 flow, which we called AVGtime. We also concluded that oxygen concentration can be calculated using temperature (K) and the AVGtime. We also concluded that O_2 does not have a significant relationship with Kelvin temperature (−.012) or with AVGtime (.022), that oxygen measurement is independent of flow, and that O_2 is not correlated with flow (.040). In our conclusions, we also found that flow is proportional to the difference between the travel time of the sound wave with and against flow ($T_{against} - T_{with}$), that flow and time with correlate inversely (−.186) at the .01 level of significance, and that flow and time against correlate (.233) at the .01 level of significance. Although we originally assumed that flow measurement would be independent of temperature, this does not seem to be correct in that flow and temperature in Kelvin and Celsius do not have a significant relationship (−.065) and flow and Δtime are highly correlated (.993). This makes sense because Boyle's law states that the volume of a gas at constant temperature is inversely proportional to the pressure to which it is subjected: $P1/P2 = V2\ V1$.

These statistical relationships above have been reinforced by our Kalman fuzzy logic, neural network, and NN supporting results. All of these results show the importance of temperature for oxygen concentration levels. The Kalman filter was shown to improve fault tolerance in the CPAP system and to help reduce failures. Our experiments also show that oxygen concentration is dependent on a specific combination of time, flow, and temperature to deliver the required O_2 to the CPAP device.

CONFLICTS OF INTEREST

None declared.

ORCID

James A. Rodger http://orcid.org/0000-0002-4580-3902

REFERENCES

Aci, M., Inan, C., & Avci, M. (2010). A hybrid classification method of k nearest neighbor, Bayesian methods and genetic algorithm. *Expert Systems with Applications*, *37*, 5061–5067.

Ammar, S., Wright, R., & Selden, S. (2000). Ranking state financial management: A multilevel fuzzy rule-based system. *Decision Sciences*, *31*, 449–481.

Andrade, R. G. S., Madeiro, F., Piccin, V. S., Moriya, H. T., Schorr, F., Sardinha, P. S., … Lorenzi-Filho, G. (2016). Impact of acute changes in CPAP flow route in sleep apnea treatment.

Aviv, Y., & Federgruen, A. (1999). The value iteration method for countable state Markov decision processes. *Operations Research Letters*, *24*, 223–234.

Aziz, A. M. (2014). A new adaptive decentralized soft decision combining rule for distributed sensor systems with data fusion. *Information Sciences*, *256*, 197–210.

Bahamon, N., Aguzzi, J., Bernardello, R., Ahumada-Sempoal, M.-A., Puigdefabregas, J., Cateura, J., … Cruzado, A. (2011). The new pelagic Operational Observatory of the Catalan Sea (OOCS) for the multisensor coordinated measurement of atmospheric and oceanographic conditions. *Sensors*, *11*, 11251–11272.

Banerjee, T. P., & Das, S. (2012). Multi-sensor data fusion using support vector machine for motor fault detection. *Information Sciences*, *217*, 96–107.

Bertram Tan, L. C., & Hsieh, P.-J. (2005). Application of the fuzzy weighted average in strategic portfolio management. *Decision Sciences*, *36*, 489–511.

Bhaskar, T., Pal, M., & Pal, A. A. (2010). Heuristic method for RCPSP with fuzzy activity times. *EJOR*, *208*, 57–66.

Bhattacharyya, S., & Pendharkar, P. C. (1998). Inductive, evolutionary, and neural computing techniques for discrimination: A comparative study. *Decision Sciences*, *29*, 871–899.

Castillo, O., Melin, P., Ramírez, E., & Soria, J. (2012). Hybrid intelligent system for cardiac arrhythmia classification with fuzzy k-nearest neighbors and neural networks combined with a fuzzy system. *Expert Systems with Applications*, *39*, 2947–2955.

Chen, C.-C., Chen, C.-L., & Lin, Y. (2016). All-digital time-domain CMOS smart temperature sensor with on-chip linearity enhancement. *Sensors*, *16*, 176. https://doi.org/10.3390/s16020176

Chen, H., Huang, C., Yu, X., Xu, X., Sun, X., Wang, G., & Wang, S. (2013). An efficient diagnosis system for detection of Parkinson's disease using fuzzy k-nearest neighbor approach. *Expert Systems with Applications*, *40*, 263–271.

Chien, C.-F., Hsu, C.-Y., Morrison, J. R., & Dou, R. (2016). Semiconductor manufacturing intelligence and automation. *Computers & Industrial Engineering*, *99*, 315–317.

Cui, L., & Murray, E. P. (2015). Effect of electrode configuration on nitric oxide gas sensor behavior. *Sensors*, *15*, 24573–24584. https://doi.org/10.3390/s150924573

Elfaki, A. O. (2016). A rule-based approach to detect and prevent inconsistency in the domain-engineering process. *Expert Systems*, *33*(1), 3–13.

Eom, K. H., Lee, S. J., Kyung, Y. S., Lee, C. W., Kim, M. C., & Jung, K. K. (2011). Improved Kalman filter method for measurement noise reduction in multi sensor RFID systems. *Sensors*, *11*, 10266–10282. https://doi.org/10.3390/s111110266

Fleming, W. H. (1966). Duality and a priori estimates in Markovian optimization problems. *Journal of Mathematical Analysis and Applications*, *16*, 254–279.

García-Pedrajas, N., & Ortiz-Boyer, D. (2009). Boosting k-nearest neighbor classifier by means of input space projection. *Expert Systems with Applications*, *36*, 10570–10582.

Govindarajan, M., & Chandrasekaran, R. M. (2010). Evaluation of k-nearest neighbor classifier performance for direct marketing. *Expert Systems with Applications*, *37*, 253–258.

Guillén-Bonilla, H., Flores-Martínez, M., Rodríguez-Betancourtt, V.-M., Guillen-Bonilla, A., Reyes-Gómez, J., Gildo-Ortiz, L., … Santoyo-Salazar, J. (2016). A novel gas sensor based on mgsb2o6 nanorods to indicate variations in carbon monoxide and propane concentrations. *Sensors*, *16*, 177. https://doi.org/10.3390/s16020177

Hall, D. L. (1992). *Mathematical techniques in multisensor data fusion*. Norwood, MA, USA: Artech House Inc.

Hewidy, A. A., Suliman, L. A., El Hefnawy, E., & Hassan, A. A. (2016). Immediate continuous positive airway pressure (CPAP) therapy after sleeve gastrectomy. *Egyptian Journal of Chest Diseases and Tuberculosis*, *65*, 701–706.

Hsieh, M.-C., Cheng, C.-Y., Liu, M.-H., & Chung, Y.-C. (2016). Effects of operating parameters on measurements of biochemical oxygen demand using a mediatorless microbial fuel cell biosensor. *Sensors*, *16*, 35. https://doi.org/10.3390/s16010035

Iftikhar, I. H., Bittencourt, L., Youngstedt, S. D., Ayas, N., Cistulli, P., Schwab, R., … Magalang, U. J. (2016). Comparative efficacy of CPAP, MADs, exercise-training and dietary weight loss for sleep apnea: A network meta-analysis. *Sleep Medicine*.

Im, J., Sterner, E. S., & Swager, T. M. (2016). Integrated gas sensing system of SWCNT and cellulose polymer concentrator for benzene, toluene, and xylenes. *Sensors*, *16*, 183. https://doi.org/10.3390/s16020183

Jain, A. K., & Dubes, R. C. (1988). *Algorithms for clustering data*. Englewood Cliffs, NJ, USA: Prentice Hall.

Jiang, S., Pang, G., Wu, M., & Kuang, L. (2012). An improved k-nearest-neighbor algorithm for text categorization. *Expert Systems with Applications*, *39*, 1503–1509.

Jiang, X., Kim, K., Zhang, S., Johnson, J., & Salazar, G. (2014). High-temperature piezoelectric sensing. *Sensors*, *14*, 144–169. https://doi.org/10.3390/s140100144

Jureschi, C.-M., Linares, J., Boulmaali, A., Dahoo, P. R., Rotaru, A., & Garcia, Y. (2016). Pressure and temperature sensors using two spin crossover materials. *Sensors*, *16*, 187. https://doi.org/10.3390/s16020187

Kao, C., & Lin, P. (2011). Qualitative factors in data envelopment analysis: A fuzzy number approach. *EJOR*, *211*, 586–593.

Klein, L. A. (2004). *Sensor and data fusion: A tool for information assessment and decision making*. Bellingham, WA, USA: SPIE Press.

Kobayashi, T., Simon, D., & Litt, J. (2005). Application of a constant gain extended Kalman filter for in-flight estimation of aircraft engine performance parameters. in Proceedings of the Turbo Expo, Reno, Nevada, USA, 6–9 June 2005; *American Society of Mechanical Engineers*.

Kurtis, R. (2016). Speed of sound in a gas. http://www.school-for-champions.com/science/sound_speed_gas.htm

Lee, C., Lin, W., Chen, Y., & Kuo, B. (2011). Gene selection and sample classification on microarray data based on adaptive genetic algorithm/k-nearest neighbor method. *Expert Systems with Applications*, *38*, 4661–4667.

Lee, P. H., & Hwang, S. S. (2009). Performance characteristics of a PEM fuel cell with parallel flow channels at different cathode relative humidity levels. *Sensors*, *9*, 9104–9121. https://doi.org/10.3390/s91109104

Li, D., Gu, H., & Zhang, L. (2010). A fuzzy c-means clustering algorithm based on nearest-neighbor intervals for incomplete data. *Expert Systems with Applications*, *37*, 6942–6947.

Li, F., Wei, Y., Chen, Y., Li, D., & Zhang, X. (2015). An intelligent optical dissolved oxygen measurement method based on a fluorescent quenching mechanism. *Sensors*, *15*, 30913–30926. https://doi.org/10.3390/s151229837

Li, H., Ji, H., Huang, Z., Wang, B., Li, H., & Wu, G. (2016). A new void fraction measurement method for gas–liquid two-phase flow in small channels. *Sensors*, *16*, 159. https://doi.org/10.3390/s16020159

Logroño, W., Guambo, A., Pérez, M., Kadier, A., & Recalde, C. (2016). A terrestrial single chamber microbial fuel cell-based biosensor for biochemical oxygen demand of synthetic rice washed wastewater. *Sensors*, *16*, 101. https://doi.org/10.3390/s16010101

Løkke, M. M., Seefeldt, H. F., Edwards, G., & Green, O. (2011). Novel wireless sensor system for monitoring oxygen, temperature and respiration rate of horticultural crops post harvest. *Sensors*, *11*, 8456–8468. https://doi.org/10.3390/s110908456

Niu, W.; Zhu, J.; Gu, W.; Chu, J. Four statistical approaches for multisensor data fusion under non-Gaussian noise . Proceedings of the 2009 IITA International Conference on Control, Automation and Systems Engineering, 2009; pp. 27–30.

Qi, J., Hu, J., & Peng, Y. (2012). A new adaptation method based on adaptability under k-nearest neighbors for case adaptation in case-based design. *Expert Systems with Applications*, *39*, 6485–6502.

Rumelhart, D. E., Hinton, G. E., & William, R. J. (1986). Learning internal representations by error propagation. In D. E. Rumelhart, & J. L. McClelland (Eds.), *Parallel distributed processing: Exploration in the microstructure of cognition: Foundations*. Cambridge, MA, USA: MIT Press. Volume 1

Skinner, H. (1979). Dimensions and clusters: A hybrid approach to classification. *Applied Psychological Measurement*, *3*, 327–341.

Soner, H. M. (1993). Motion of a set by the curvature of its boundary. *Journal of Differential Equations*, *101*, 313–372.

Stratulat, A., Serban, B.-C., de Luca, A., Avramescu, V., Cobianu, C., Brezeanu, M., … Udrea, F. (2015). Low power resistive oxygen sensor based on sonochemical SrTi0.6Fe0.4O2.8 (STFO40). *Sensors*, *15*, 17495–17506. https://doi.org/10.3390/s150717495

Tang, F., Wang, X., Wang, D., & Li, J. (2008). Non-invasive glucose measurement by use of metabolic heat conformation method. *Sensors*, *8*, 3335–3344. https://doi.org/10.3390/s8053335

Wang, H., Chen, L., Wang, J., Sun, Q., & Zhao, Y. (2014). A micro oxygen sensor based on a nano sol–gel TiO_2 thin film. *Sensors*, *14*, 16423–16433. https://doi.org/10.3390/s140916423

Wang, H., Liu, X., Pedrycz, W., Zhu, X., & Hu, G. (2011). Mining axiomatic fuzzy set association rules for classification problems. *EJOR*.

Wang, J., & Liang, K. (2008). Multi-sensor data fusion based on fault detection and feedback for integrated navigation systems. Proceedings of the International Symposium on Intelligent Information Technology Application Workshops, pp. 232–235.

Weiss, S. M., & Kapouleas, I. (1989). An empirical comparison of pattern recognition, neural nets, and machine learning classification methods. Proceedings of the Eleventh International Joint Conference on Artificial Intelligence, Detroit, MI, USA, Morgan Kaufmann: Los Altos, CA, USA, pp. 688–693.

Yager, R. (1981). Concepts, theory, and techniques: A new methodology for ordinal multiobjective decisions based on fuzzy sets. *Decision Sciences*, *12*, 589–600.

Zhang, C., & Wang, H. (2010). Decentralized multi-sensor data fusion algorithm using information filter. Proceedings of the International Conference on Measuring Technology and Mechatronics Automation, pp. 890–893.

Zhu, H., Leung, H., & He, Z. (2013). A variational Bayesian approach to robust sensor fusion based on Student-*t* distribution. *Information Sciences*, *221*, 201–214.

James A. Rodger is a Professor of Management Information Systems and Decision Sciences at Indiana University of Pennsylvania (IUP). He received his doctorate in MIS from Southern Illinois University at Carbondale in 1997. Dr. Rodger has published several journal articles related to these subjects. His work has appeared in the following journals: *Journal of Computer Information Systems*, *Issues in Information Systems*, *IEEE Transactions on Software Engineering*, *International Journal of Hybrid Intelligent Systems*, *Information and Software Technology*, *Information Technology and Management*, *Annals of Operations Research*, *Communications of ACM*, *Computers & Operations Research*, *Decision Support Systems*, *Expert Systems with Applications*, *Lecture Notes in Computer Science*, and *International Journal of Human-Computer Studies* as well as several other journals.

How to cite this article: Rodger JA. Advances in multisensor information fusion: A Markov–Kalman viscosity fuzzy statistical predictor for analysis of oxygen flow, diffusion, speed, temperature, and time metrics in CPAP. *Expert Systems*. 2018;35:e12270. https://doi.org/10.1111/exsy.12270